Immunoglobulin G1 Fc domain motions: implications for Fc engineering

Martin Frank[1], **Ross C. Walker**[2], **William N. Lanzilotta**[3], **James H. Prestegard**[4], and **Adam W. Barb**[5,*]

[1]Biognos AB, Generatorsgatan 1, 41705 Gothenburg, Sweden

[2]San Diego Supercomputer Center and Department of Chemistry and Biochemistry, University of California, San Diego, La Jolla, California 92093, United States

[3]Department of Biochemistry and Molecular Biology, University of Georgia, Athens GA 30602

[4]Complex Carbohydrate Research Center, University of Georgia, Athens GA 30602

[5]Roy J. Carver Department of Biochemistry, Biophysics and Molecular Biology, Iowa State University, Ames, IA 50011

Abstract

The fragment crystallizable (Fc) region links the key pathogen identification and destruction properties of immunoglobulin G(IgG). Pathogen opsonization positions Fcs to activate pro-inflammatory Fcγ receptors (FcγRs) on immune cells. The cellular response and committal to a damaging, though protective, immune response is tightly controlled at multiple levels. Control mechanisms are diverse and in many cases unclear, but one frequently suggested contribution originates in Fcγ receptor affinity being modulated through shifts in Fc conformational sampling. Here we report a previously unseen IgG1 Fc conformation. This observation motivated an extensive molecular dynamics (MD) investigation of polypeptide and glycan motions that revealed greater amplitude of motion for the N-terminal Cγ2 domains and N-glycan than previously observed. Residues in the Cγ2/Cγ3 interface and disulphide-bonded hinge were identified as influencing the Cγ2 motion. Our results are consistent with a model of Fc that is structurally dynamic. Conformational states that are competent to bind immune-stimulating FcγRs interconverted with Fc conformations distinct from those observed in FcγR complexes, which may represent a transient, nonbinding population.

---

*Correspondence: abarb@iastate.edu; (515)-294-8928; 2214 MBB, Iowa State University, Ames, IA 50011.

Introduction

The adaptive immune system floods the serum with pathogen-specific immunoglobulin G (IgG) antibodies (5–15 mg / mL) to protect against infection [1]. The antigen-binding Fab domains of IgG are responsible for specificity. Once engaged, however, the Fragment crystallizable (Fc) region of IgG initiates the classical complement pathway or cellular-mediated target destruction through interactions with immune cell receptors. Aside from its natural function, the IgG system itself has been appropriated in the treatment of autoimmune disorders [2], and a number of synthetic antibodies have been designed to sequester soluble proteins implicated in other diseases or recognize cancerous tissue [3; 4]. Despite this utility, the atomic-level structural factors governing particularly the Fc-mediated immune response remain unclear. Marked improvements in therapeutic antibody efficacy, pharmacokinetics and production could clearly result from a more complete description of these factors. Here we present structural data from X-ray crystallography and extensive MD simulations that is relevant to this issue.

The Fc portion of IgG is a homodimer formed by the C-terminal halves of the IgG heavy chains; the monomers are covalently linked by a disulphide 'hinge' region that remains intact following papain protease digestion to liberate Fab fragments (Figure 1). Each Fc monomer is composed of Cγ2 (N-terminal) and Cγ3 (C-terminal) domains. In addition to the hinge disulphides at the N-terminus of the Cγ2 domain, a non-covalent Cγ3 / Cγ3 polypeptide interface links the C-terminal region. Each Fc polypeptide contains a single conserved and essential asparagine(297)-linked complex-type biantennary glycan (N-glycan; Fig. 1B) [5]. The N-glycan had been shown to reside within a cavity between the Fc polypeptide monomers [6] and was initially believed to be stably bound in this location. However, given this model it was unclear why the N-glycan was sensitive to glycosylhydrolases and glycosyltransferases [7–9] until nuclear magnetic resonance spectroscopy (NMR) measurements of the terminal glycan residues provided clear evidence for unbound conformations [10; 11].

The N-glycans are essential to proper Fc function and antibody dependent cellular cytotoxicity [12]. Particular glycoforms are also known to modulate immune responses and alter stability of therapeutic antibodies [5; 13–15]. However, it is not entirely clear how these effects arise. Recent structures of the Fc - FcγRIIIa complex showed the monomeric receptor bound asymmetrically to the Cγ2 domains of the Fc dimer near the hinge [16–18]. This is intriguing because it is known that changes at the glycan termini affect Fc - FcγRIIIa affinity [17; 19; 20], despite the fact that glycan termini are far away from the site of receptor binding (Figure 1). A possible explanation, based on x-ray crystallography-derived structures, is that the N-glycan termini mediate affinity by modulating the Cγ2 domain positions and thus the organization of the FcγRIIIa binding site [19]. The various structures of Fc and its complexes provide some indication of Fc conformational heterogeneity, though it is unclear whether the complete range of Fc motion is sampled. An understanding of these motions would provide a more complete view of IgG behavior in solution and the factors contributing to FcγRIIIa-mediated immune activation.

Our goal is to describe the factors that influence IgG-mediated immune activation, starting with this investigation of Fc conformation sampling. The crystal structure we obtained using a single homogenous glycoform terminated with galactose (Gal) on each of the branches of the biantennary N-glycans extends the range of conformers observed in structures for similar constructs. Prompted by the observation of this new conformational form, we performed all-atom simulations of the Fc and probed the factors that contribute to Fc motion.

Results

X-ray crystallography

Crystals from a number of different PEG-based conditions produced moderate to high-resolution datasets, with the polypeptide and glycan chains clearly resolved. However, crystals from only one condition diffracted to greater than 2.0 Å resolution, and these crystals revealed a previously unobserved conformation (Figure 1A). Refinement of this structure was pursued and crystallographic statistics are given in Table 1.

A comparison of the refined structure and Fc structures from the protein data bank (PDB[21]) containing similarly remodeled Gal-terminated N-glycans revealed striking differences in the orientation of the Cγ2 domains (Figure 2A). The positions of both Cγ2 domains in our structure were outliers when compared to other Fc structures (Fig. 2B) and were suggestive of a greater degree of Fc conformational heterogeneity within a single glycoform than previously observed. A similar, though slightly greater, range of Cγ2 positions was found upon comparison to a broader sampling of Fc structures from the database, which included the presence of other glycan types and, in a few cases, Fc-binding polypeptides (Fig. 1 B&D).

A complete analysis of the domain orientation angles and distances is shown in Table 2. For purposes of quantitation, alignments were generated using the Cγ3/ Cγ3 dimer portion of the models due to the high similarity across all models (<0.5 Å rmsd). Three point angles were then defined from the Cα atoms of residues Y300, M428 and Q362 for Cγ2 / Cγ3 angles or M428 (chain A), Q362 (chain A) and M428 (chain B) for Cγ3 (chain A)/ Cγ3 (chain B) angles. Four point dihedral angles were defined from the Cα atoms of residues Y300, Y319, M428 and Q362 for Cγ2 / Cγ3 dihedral angles or M428 (chain A), Q362 (chain A), Q362 (chain B) and M428 (chain B) for Cγ3 (chain A)/ Cγ3 (chain B) dihedral angles. Cγ2 interdomain distances were represented by the distance between the α-carbons of Asn297 where the glycans are attached. Among the structures with homogenous Gal terminated glycans, ours has the largest Cγ2 / Cγ3 dihedral angle (−31.1° compared to a previous range of −20.4 to −30.5) and the smallest Cγ2-Cγ2 distance (29.1 Å compared to a previous range of 32.2–33.3 Å). Considering all glycoforms and other types of complexes, ranges expand to encompass the values we observe (−20.4 to −33.4° and 22.8 to 36.2 Å). Different reference points for the Cγ2 / Cγ 3 angle and Cγ2 - Cγ2 distance were noted previously[22] and are shown for comparison in Table S1. Our structure also gives a good view of glycan position and interaction, particularly for the α1–6Man-linked branch (Figure S1).

Computational Modeling of Fc conformation

It is unclear whether the range of distinct Fc conformational states is limited by crystal contacts or alternative states are sampled in solution. Therefore we probed the range of Fc polypeptide and glycan motions using extended, all-atom computational simulations of Fc with Gal-terminated glycans and an intact hinge region (which was present, though not necessarily resolved, in all the Fc models used for Table 2). Our new structure served as a computational starting point and revealed that the unique conformation observed by x-ray crystallography, like many other database models, was only lightly populated during the MD simulation. However, this unique conformation was preserved in a simulation of the starting model confined within the crystalline lattice (data not shown), indicating this state, and likely many others determined by x-ray crystallography, is restrained by crystal lattice contacts.

Extensive 200 ns simulations of Fc motions relieved of solid state contacts and initialized with a database model including hinge coordinates (pdb 3SGJ [18]) provided an indication of Fc motions (Fig 3A). The Cγ2 domains opened and closed at the hinge region and sampled a range of conformations not seen through x-ray crystallography. MD simulations, such as this, offer insight into macromolecular flexibility but fall short of complete descriptions of motion due to computational limits (extensive μs to ms simulations are currently not practical for systems of this size). Furthermore, rates of motion and population distributions are likely not accurately reproduced in silico. However, we believe this 200 ns simulation provides a limited, though likely appropriate, view of sampled states. Given the limited timescale of simulations, it is unlikely that the MD over predicts flexibility. Future experiments in solution may well provide validation of rates of motion, amplitudes, and most favored orientations for Cγ2/3 as presented below, though this lies at the cutting edge of contemporary structural biology due to the size and complexity of this system.

The range of Cγ2 / Cγ3 domain orientation angles sampled in the simulation (75° to 108°) was greater than that of the database models (91° to 104°) (Fig. 3B and Table 2). Furthermore, the database models populated the high end of the MD distribution. The dihedral angle, describing the twist of Cγ2 relative to Cγ3, showed variability with the simulation range (−46° to 5°) greater than the database models (−33° to −20°). The Cγ2-Cγ2 distance variation sampled was substantially larger than that sampled by crystallography of Fc with Gal terminated glycans and similar to that seen for the entire set of Fc structures. The variability of the Cγ3 / Cγ3 angle and dihedral angle, as expected, was markedly less than those for Cγ2 / Cγ3 (Figure S2).

Further analysis of Fc from MD and database models revealed more differences. The conformations most frequently sampled by MD (~87° angle, −15-−25° dihedral) are not coincident with conformations of the database models including those bound to FcγRIIIa (Fig 3B). Assuming these simulations faithfully recapitulate solution behavior, this suggests two possibilities: Gal-Fc in solution is not perfectly poised to bind FcγRIIIa, or crystal contacts distort Fc conformation in the complex, as observed for unliganded Fc. Perhaps simulations of Fc with GlcNAc- or Man-terminated glycans (thought to bind weaker to FcγRIIIa[23]) or the Fc–FcγRIIIA complex will reveal conformations more similar to the database models.

Analysis of carbohydrate motions

Terminal carbohydrate residues experience considerable motion relative to the polypeptide, based on previous experimental results [10; 11]. Specifically, these prior studies showed the α1-6Man-linked branch of the complex-type, biantennary glycan (Fig. 1B) exchanged between free and bound conformations, while the (α1-3Man-linked)Gal residues appeared unconstrained by polypeptide contacts. Gal behavior in the computational simulations presented here was qualitatively consistent with published results in that the (α1-6Man-linked) Gal residues occasionally lifted off the protein surface and exhibited enhanced motion. A range of carbohydrate structures was observed as highlighted in Figure 4. Both (α1-6Man-linked) Gal residues occupied polypeptide bound (<9 Å, as defined by the Pro244 Cα–Gal C1 distance in Figure 4B) and unbound states (>9 Å). The partial occlusion of the Gal-polypeptide interface by movement of the Glu258 carboxylate at some times explained the presence of two discrete bound Gal states occurring at ~6 and ~8 Å. The behavior of this Gal residue, under conditions explored in simulations reported here, appeared decoupled from Cγ2 /Cγ3 motions, as might be expected as both the attachment site and the terminal glycan binding region reside within the same Cγ2 domain. It is possible that interactions leading to correlated motions could occur as with long time scale excursions completely outside the cavity. Such excursions must occur to allow enzyme modification of glycan termini.

Analysis of glycosidic torsion angles revealed a strong correlation with glycan bound and unbound states. Gal and GlcNAc residues on the glycan branch termini showed similar conformational distributions that compared favorably to identical motifs in the PDB with the exception of the α1-6Man-linked residues of chain B which had comparatively restricted distributions (Figure 5). Torsion angles of the core Fuc, α1-3Man and βMan residues showed a similar pattern suggesting linkage and residue identities influenced conformation to a greater extent than polypeptide interactions with the exception of α1-6Man-linked residues on chain B which, like the chain B Cγ2 domain (Fig 4B, 5C, 6A&C), was likely more restricted due to contacts with the asymmetrically disposed hinge region populated in the MD simulations (not shown). This asymmetry likely reflects the limited sampling of the simulation compared to the timescale required for a conformational change of the hinge (Fig 3B). Over long times it is expected that the hinge is distributed equally towards chain A and chain B due to the dimer symmetry of the system. The ω torsion angle of the α1-6Man residue, however, showed a clear correlation with the glycan state. The chain A α1-6Man ω torsion angle shifted to 180° from −60° ~65 ns into the simulation, and did not return (Fig 4C). In the simulation snapshots with a 180° ω angle were unbound for 70% of the time compared to 2% for frames with a −60° ω angle (Fig. 4 B&C).

The role of the hinge and interface

The role of motion-restricting Fc amino acid residues was probed in silico. The hinge region was identified as a target for mutation due to the presence of the potentially conformationally-restricting interdomain covalent bonds. Surprisingly a 200 ns simulation of Fc without 10 N-terminal hinge residues (and the two disulphide bonds as shown in Figure 7A–C) behaved similarly to the wild type (wt) Fc, though one Cγ2 domain did collapse onto the Cγ3 (observed for the small Cγ2 / Cγ3 angle structures in Fig. 7B). The

greatest difference was observed in the Cγ2 / Cγ3 angles with a slight displacement to smaller values and a slightly broader distribution in the hinge-deletion simulation (81.6° ±7.9° compared to 89.6°±3.9° (±one standard deviation of the mean) for the wt simulation, Fig. 7 A–C). Simulations of Fc mutated to disrupt two ionic interactions across the Cγ2 / Cγ3 interface (Glu380Ala, Glu430Ala) likewise showed a greater distribution of Cγ2 / Cγ3 angles (89.5°±8.8°) as well as limited sampling of extended structures (Fig. 7 D–F). Also, multiple small, <5 Å, reversible interface breaks were observed in multiple simulations (Figure 7D–F) and supported the role of Glu380 and Glu430 in Fc conformational stability. The Cγ2 domains of hinge deleted and Glu mutated Fc were considerably less restricted (112.3°±15.9°, Fig. 7G–I) in additional simulations, indicating the importance of both regions in limiting Cγ2 motion. These extensive simulations provide clues to Cγ2 motions, however, the actual range of wt and mutant Fc motions will be the subject of further in vitro experimental studies.

Discussion

These studies highlight previously unseen Fc domain conformations and motions. This is primarily due to the fortuitous recovery of a new Fc crystalline form and the accessibility of computational tools to investigate large glycoproteins with appropriate force fields over relatively long timescales. There is no doubt that Fc motions remain undersampled. Efforts to describe the actual range of wt and mutant Fc will be the subject of future accelerated molecular dynamics simulations and solution NMR studies. Despite this limitation, the range of motion described here expands our understanding of conformations that can be sampled in solution.

Fc domain motions

In MD simulations, the Cγ2 domains experienced greater amplitude of motion than anticipated once relieved of crystal contacts. Though multiple studies have revealed new conformations of Fc built from x-ray diffraction data and mutant Fcs (for example, but not limited to [22; 24–29]), in this study we focused on those reported for human IgG1 Fc having Gal-terminated N-glycans and human IgG1 Fc in complex with the FcγR, with the goal of thoroughly characterizing appropriate Fc motions.

The implications of greater motion for FcγR binding can be many. However, the sampling does indicate that there are a range of low energy conformers from which various Fcγ receptors can choose. It is possible that conformer populations are tuned by glycoform selection to produce desirable receptor affinities, and thus an important regulatory mechanism. The immune system must walk a fine line between defensive response and harmful auto-immune reactions. High affinity interactions could be undesirable and lead to spurious FcγR-mediated activation. On the other hand, low affinity could be overcome upon proper presentation of Fcs by multiple antibodies on an opsonized pathogen, due primarily to multivalency (high avidity) effects. It has been suggested that the sugars at the N-glycan termini influence the Fc structure through the Cγ2 domain orientation and thus receptor binding [19]. We would simply add that it may not be static structural perturbations that are

primary effectors of this phenomenon, but rather the glycan regulates the range of structures sampled, and thus the population of FcγR-binding-competent Fc conformations.

If Cγ2 motions are an important component of FcγR-mediated immune activation, the genetically-encoded Fc features contributing to this interaction may be investigated, and perhaps engineered. The results of our simulations identify both the disulphide-bonded hinge region and the Cγ2 / Cγ3 interface as important regulators of Fc motion. The hinge disulphides likely restrict the range of Cγ2 motions by acting as a tether, though it was surprising that hinge deletion didn't more dramatically alter Fc motions. The hinge works in concert with the Cγ2 / Cγ3 interface, which upon inspection, is a poorly defined interface with little buried surface area and few hydrophobic interactions, but with two Lys$^+$-Glu$^-$ ionic interactions that are stable throughout almost the entire wt Fc simulation (data not shown). It appears that perturbing this interface influences Cγ2 position, particularly in the absence of the hinge. A recent study of human IgG2 Fc showed similar interface behavior [30]. This is intriguing because interface mutations to stabilize Fc in an FcγR-binding conformation should dramatically alter the effector functions of Fc. This has obvious implications for therapeutic monoclonal antibody design and would be independent of the hinge.

N-glycan motions

The motion of the carbohydrate in the computational simulation was qualitatively consistent with expectation based on NMR measurements [10; 11]. The (α1-6Man-linked)Gal residues on both chains experienced conformations bound to the polypeptide surface as well as free from this restriction (Figure 4). However, the free form of the glycan still appears sterically restricted from enzymatic modification, due to a location in the cavity between polypeptide domains, and thus a complete quantitiative analysis of glycan populations using these data is not appropriate. This may simply be due to computational limitations. NMR evidence suggested the exchange of the two glycan states to occur with a half-life of hundreds of μs [10], which was obviously not sampled with the relatively short 200 ns simulation. Directed molecular dynamics simulations, accelerated molecular dynamics approaches [31] or simulations beginning with starting conformations chosen using appropriate sampling algorithms might provide greater insight into the complete ensemble of Fc N-glycan motions, as well as that of the peptide domains which seem to confine them.

That the α1-6Man branch of a biantennary N-glycan experiences greater conformational heterogeneity than the α1-3Man branch of the glycan is expected based on the presence of an additional glycosidic torsion angle (ω)[32]. Thus, if restricting the Fc N-glycan is necessary for effective FcγRIIIa binding, a conformationally-constraining interaction between the Fc polypeptide and its glycan through the α1-6Man-linked branch is poised to provide the greatest total glycan restriction with the smallest possible interface. In another sense, coordinating the α1-6 branch terminus is an efficient way to restrict an entire biantennary N-glycan.

Experimental Procedures

Materials

All materials were purchased from Sigma Aldrich (St. Louis, MO), unless otherwise noted.

Protein crystallization, model building and refinement

Fc from pooled human serum (Athens Research and Technology, Athens, Georgia) was remodeled to display Gal-terminated, core fucosylated glycans as previously described [9]. Protein was purified following glycan remodeling using a Protein A resin (GE Healthcare) and eluted with 100 mM Glycine, pH 3.0. Fractions were immediately neutralized with 100 mM Tris pH 8.0 and buffer exchanged to 25 mM MOPS, 100 mM KCl, pH. 7.2. Protein was concentrated to 16 mg/mL using a 10 kDa molecular weight cutoff centrifugal unit (Millipore).

The PEGRx™ screens 1 and 2 (Hampton Research, Aliso Viejo CA) were assayed for crystallization by diluting the protein solution (1 μL) with reagent (1 μL) and suspending the drop on a glass coverslip over 1 mL of reagent. Crystallization trays were incubated at 25 °C. Large, high-quality crystals typically appeared within five days, were excised and transferred to a cryo-compatible liquor by stepwise addition of PEG 200 (2.5 % increments) to 10 % and flash frozen in liquid nitrogen. Protein crystals with favorable diffraction characteristics were found using a reagent containing 0.1 M Sodium acetate, pH 6.5 and 30 % (w/v) polyethylene glycol 1,500.

Data were collected at the Advanced Light Source through SER-CAT on the beam line 22-BM. Data indexing, integration and scaling were performed with HKL2000 [33] and initial phases were obtained by molecular replacement using a poly-alanine model of chain A from an existing model of the human Fc fragment (1L6X). After a reasonable solution was identified, a composite omit map was generated using the simulated annealing protocol and the model and map were inspected. All residues that did not correlate with electron density were removed and iterative rounds of model building and refinement were carried out using the programs COOT [34] and CNS [35], respectively. The final round of refinement and the final model was prepared for deposition using CCP4 [36].

Molecular Dynamics Simulations

The starting structures were built based on our new crystal structure and pdb entry 3SGJ [18]. Monosaccharide rings having distorted ring geometries were assigned a $^4C_1$ chair conformation and missing terminal Gal residues were added to initialization models prior to generating a topology file for AMBER 12 using the tleap tool [37; 38]. The AMBER ff99SB [39] force field was used for the protein and carbohydrate parameters were taken from the GLYCAM06 force field [40]. The glycoprotein was solvated in a box of TIP3P water with approximate dimensions 91 Å × 91 Å × 91 Å using periodic boundary conditions. A two step energy minimization was carried out for removal of initial unfavorable contacts followed by heating the system slowly from 5 to 310 K for 100 ps in the canonical NVT ensemble, followed by 100 ps at constant temperature of 310 K and constant pressure of 1 atm. Starting structures for the MD simulations of the glycoprotein variants with mutations

and/or hinge-deletion were prepared and equilibrated in an analogous manner. Production dynamics of the 200 ns wild type Fc simulation was performed using PMEMD using 96 CPUs of the NSF Kraken Cray XT4 supercomputer at 310 K with snapshots recorded every 20 ps. The other production simulations were run on NVIDIA Tesla C2070 GPUs using the GPU accelerated version of the AMBER 12 PMEMD software [41–43]. The time step used for all stages was 2 fs and all hydrogen atoms were constrained using the SHAKE algorithm [44]. Long-range electrostatics were included using the Particle Mesh Ewald algorithm [45]. Structural snapshots were recorded every 2 ps. Molecular dynamics trajectories were analyzed using Conformational Analysis Tools (www.md-simulations.de/CAT/) and VMD [46]. Structure images were prepared with VMD or Pymol (The PyMOL Molecular Graphics System, Version 1.5.0.5 Schrödinger, LLC). Glycan torsion angles from the PDB were obtained using the GlyTorsion functionality on the Glycosciences (www.glycosciences.de) website[47]. Averaging over 10 frames reduced noise in the plotted trajectories. Duplicate simulations gave similar results (data not shown).

Supplementary Material

Refer to Web version on PubMed Central for supplementary material.

Acknowledgments

References

1. Janeway, C.; Murphy, KP.; Travers, P.; Walport, M. Janeway's immuno biology. 7. Garland Science; New York: 2008.

2. Schwab I, Nimmerjahn F. Intravenous immunoglobulin therapy: how does IgG modulate the immune system? Nat Rev Immunol. 2013; 13:176–89. [PubMed: 23411799]

3. Stern M, Herrmann R. Overview of monoclonal antibodies in cancer therapy: present and promise. Crit Rev Oncol Hematol. 2005; 54:11–29. [PubMed: 15780905]

4. Dubel S. Recombinant therapeutic antibodies. Appl Microbiol Biotechnol. 2007; 74:723–9. [PubMed: 17225094]

5. Parekh RB, Dwek RA, Sutton BJ, Fernandes DL, Leung A, Stanworth D, Rademacher TW, Mizuochi T, Taniguchi T, Matsuta K, et al. Association of rheumatoid arthritis and primary osteoarthritis with changes in the glycosylation pattern of total serum IgG. Nature. 1985; 316:452–7. [PubMed: 3927174]

6. Deisenhofer J. Crystallographic refinement and atomic models of a human Fc fragment and its complex with fragment B of protein A from Staphylococcus aureus at 2.9- and 2.8-A resolution. Biochemistry. 1981; 20:2361–70. [PubMed: 7236608]

7. Kobata A. The N-linked sugar chains of human immunoglobulin G: their unique pattern, and their functional roles. Biochim Biophys Acta. 2008; 1780:472–8. [PubMed: 17659840]

8. Raju TS, Briggs JB, Chamow SM, Winkler ME, Jones AJ. Glycoengineering of therapeutic glycoproteins: in vitro galactosylation and sialylation of glycoproteins with terminal N-acetylglucosamine and galactose residues. Biochemistry. 2001; 40:8868–76. [PubMed: 11467948]

9. Barb AW, Brady EK, Prestegard JH. Branch-specific sialylation of IgG-Fc glycans by ST6Gal-I. Biochemistry. 2009; 48:9705–7. [PubMed: 19772356]

10. Barb AW, Prestegard JH. NMR analysis demonstrates immunoglobulin G N-glycans are accessible and dynamic. Nat Chem Biol. 2011; 7:147–53. [PubMed: 21258329]

11. Barb AW, Meng L, Gao Z, Johnson RW, Moremen KW, Prestegard JH. NMR characterization of immunoglobulin G Fc glycan motion on enzymatic sialylation. Biochemistry. 2012; 51:4618–26. [PubMed: 22574931]

12. Arnold JN, Wormald MR, Sim RB, Rudd PM, Dwek RA. The impact of glycosylation on the biological function and structure of human immunoglobulins. Annual Review of Immunology. 2007; 25:21–50.

13. Lauc G, Huffman JE, Pucic M, Zgaga L, Adamczyk B, Muzinic A, Novokmet M, Polasek O, Gornik O, Kristic J, Keser T, Vitart V, Scheijen B, Uh HW, Molokhia M, Patrick AL, McKeigue P, Kolcic I, Lukic IK, Swann O, van Leeuwen FN, Ruhaak LR, Houwing-Duistermaat JJ, Slagboom PE, Beekman M, de Craen AJ, Deelder AM, Zeng Q, Wang W, Hastie ND, Gyllensten U, Wilson JF, Wuhrer M, Wright AF, Rudd PM, Hayward C, Aulchenko Y, Campbell H, Rudan I. Loci associated with N-glycosylation of human immunoglobulin G show pleiotropy with autoimmune diseases and haematological cancers. PLoS Genet. 2013; 9:e1003225. [PubMed: 23382691]

14. Wright A, Morrison SL. Effect of altered CH2-associated carbohydrate structure on the functional properties and in vivo fate of chimeric mouse-human immunoglobulin G1. J Exp Med. 1994; 180:1087–96. [PubMed: 8064227]

15. Kanda Y, Yamada T, Mori K, Okazaki A, Inoue M, Kitajima-Miyama K, Kuni-Kamochi R, Nakano R, Yano K, Kakita S, Shitara K, Satoh M. Comparison of biological activity among nonfucosylated therapeutic IgG1 antibodies with three different N-linked Fc oligosaccharides: the high-mannose, hybrid, and complex types. Glycobiology. 2007; 17:104–18. [PubMed: 17012310]

16. Sondermann P, Huber R, Oosthuizen V, Jacob U. The 3.2-A crystal structure of the human IgG1 Fc fragment-Fc gammaRIII complex. Nature. 2000; 406:267–73. [PubMed: 10917521]

17. Mizushima T, Yagi H, Takemoto E, Shibata-Koyama M, Isoda Y, Iida S, Masuda K, Satoh M, Kato K. Structural basis for improved efficacy of therapeutic antibodies on defucosylation of their Fc glycans. Genes Cells. 2011; 16:1071–80. [PubMed: 22023369]

18. Ferrara C, Grau S, Jager C, Sondermann P, Brunker P, Waldhauer I, Hennig M, Ruf A, Rufer AC, Stihle M, Umana P, Benz J. Unique carbohydrate-carbohydrate interactions are required for high affinity binding between FcgammaRIII and antibodies lacking core fucose. Proc Natl Acad Sci U S A. 2011; 108:12669–74. [PubMed: 21768335]

19. Krapp S, Mimura Y, Jefferis R, Huber R, Sondermann P. Structural analysis of human IgG-Fc glycoforms reveals a correlation between glycosylation and structural integrity. Journal of Molecular Biology. 2003; 325:979–89. [PubMed: 12527303]

20. Kaneko Y, Nimmerjahn F, Ravetch JV. Anti-inflammatory activity of immunoglobulin G resulting from Fc sialylation. Science. 2006; 313:670–673. [PubMed: 16888140]

21. Bernstein FC, Koetzle TF, Williams GJ, Meyer EF Jr, Brice MD, Rodgers JR, Kennard O, Shimanouchi T, Tasumi M. The Protein Data Bank: a computer-based archival file for macromolecular structures. J Mol Biol. 1977; 112:535–42. [PubMed: 875032]

22. Oganesyan V, Damschroder MM, Leach W, Wu H, Dall'Acqua WF. Structural characterization of a mutated, ADCC-enhanced human Fc fragment. Mol Immunol. 2008; 45:1872–82. [PubMed: 18078997]

23. Yamaguchi Y, Nishimura M, Nagano M, Yagi H, Sasakawa H, Uchida K, Shitara K, Kato K. Glycoform-dependent conformational alteration of the Fc region of human immunoglobulin G1 as revealed by NMR spectroscopy. Biochimica Et Biophysica Acta-General Subjects. 2006; 1760:693–700.

24. Yu X, Baruah K, Harvey DJ, Vasiljevic S, Alonzi DS, Song BD, Higgins MK, Bowden TA, Scanlan CN, Crispin M. Engineering hydrophobic protein-carbohydrate interactions to fine-tune monoclonal antibodies. J Am Chem Soc. 2013; 135:9723–32. [PubMed: 23745692]

25. Crispin M, Yu X, Bowden TA. Crystal structure of sialylated IgG Fc: Implications for the mechanism of intravenous immunoglobulin therapy. Proc Natl Acad Sci U S A. 2013

26. Bowden TA, Baruah K, Coles CH, Harvey DJ, Yu X, Song BD, Stuart DI, Aricescu AR, Scanlan CN, Jones EY, Crispin M. Chemical and structural analysis of an antibody folding intermediate trapped during glycan biosynthesis. J Am Chem Soc. 2012; 134:17554–63. [PubMed: 23025485]

27. Crispin M, Bowden TA, Coles CH, Harlos K, Aricescu AR, Harvey DJ, Stuart DI, Jones EY. Carbohydrate and domain architecture of an immature antibody glycoform exhibiting enhanced effector functions. J Mol Biol. 2009; 387:1061–6. [PubMed: 19236877]

28. Nagae M, Yamaguchi Y. Function and 3D Structure of the N-Glycans on Glycoproteins. Int J Mol Sci. 2012; 13:8398–429. [PubMed: 22942711]

29. Borrok MJ, Jung ST, Kang TH, Monzingo AF, Georgiou G. Revisiting the role of glycosylation in the structure of human IgG Fc. ACS Chem Biol. 2012; 7:1596–602. [PubMed: 22747430]

30. Teplyakov A, Zhao Y, Malia TJ, Obmolova G, Gilliland GL. IgG2 Fc structure and the dynamic features of the IgG CH2-CH3 interface. Mol Immunol. 2013; 56:131–9. [PubMed: 23628091]

31. Pierce LCTSFR, Augusto F, de Oliveira C, McCammon JA, Walker RC. Routine access to millisecond timescale events with accelerated molecular dynamics. J Chem Theory Comput. 2012; 8:2997–3002. [PubMed: 22984356]

32. Salisburg AM, Deline AL, Lexa KW, Shields GC, Kirschner KN. Ramachandran-type plots for glycosidic linkages: Examples from molecular dynamic simulations using the Glycam06 force field. J Comput Chem. 2009; 30:910–21. [PubMed: 18785152]

33. Otwinowski Z, Minor W. Processing of X-ray diffraction data collected in oscillation mode. Macromolecular Crystallography, Pt A. 1997; 276:307–326.

34. Emsley P, Lohkamp B, Scott WG, Cowtan K. Features and development of Coot. Acta Crystallogr D Biol Crystallogr. 2010; 66:486–501. [PubMed: 20383002]

35. Brunger AT. Version 1.2 of the Crystallography and NMR system. Nat Protoc. 2007; 2:2728–33. [PubMed: 18007608]

36. Murshudov GN, Skubak P, Lebedev AA, Pannu NS, Steiner RA, Nicholls RA, Winn MD, Long F, Vagin AA. REFMAC5 for the refinement of macromolecular crystal structures. Acta Crystallogr D Biol Crystallogr. 2011; 67:355–67. [PubMed: 21460454]

37. Case, DA.; TAD; Cheatham, TE., III; Simmerling, CL.; Wang, J.; Duke, RE.; Luo, R.; Walker, RC.; Zhang, W.; Merz, KM.; Roberts, B.; Hayik, S.; Roitberg, A.; Seabra, G.; Swails, J.; Götz, AW.; Kolossváry, I.; Wong, KF.; Paesani, F.; Vanicek, J.; Wolf, RM.; Liu, J.; Wu, X.; Brozell, SR.; Steinbrecher, T.; Gohlke, H.; Cai, Q.; Ye, X.; Wang, J.; Hsieh, M-J.; Cui, G.; Roe, DR.; Mathews, DH.; Seetin, MG.; Salomon-Ferrer, R.; Sagui, C.; Babin, V.; Luchko, T.; Gusarov, S.; Kovalenko, A.; Kollman, PA. Amber 12. University of California; San Francisco: 2012.

38. Salomon-Ferrer R, Case DA, Walker RC. An overview of the Amber biomolecular simulation package. Wiley Interdisciplinary Reviews: Computational Molecular Science. 2013; 3:198–210.

39. Hornak V, Abel R, Okur A, Strockbine B, Roitberg A, Simmerling C. Comparison of multiple Amber force fields and development of improved protein backbone parameters. Proteins. 2006; 65:712–25. [PubMed: 16981200]

40. Kirschner KN, Yongye AB, Tschampel SM, Gonzalez-Outeirino J, Daniels CR, Foley BL, Woods RJ. GLYCAM06: A generalizable Biomolecular force field. Carbohydrates. Journal of Computational Chemistry. 2008; 29:622–655. [PubMed: 17849372]

41. Gotz AW, Williamson MJ, Xu D, Poole D, Le Grand S, Walker RC. Routine Microsecond Molecular Dynamics Simulations with AMBER on GPUs. 1. Generalized Born. J Chem Theory Comput. 2012; 8:1542–1555. [PubMed: 22582031]

42. Le Grand S, Götz AW, Walker RC. SPFP: Speed without compromise—A mixed precision model for GPU accelerated molecular dynamics simulations. Computer Physics Communications. 2013; 184:374–380.

43. Salomon-Ferrer RGAW, Poole D, Grand S, Walker RC. Routine microsecond molecular dynamics simulations with AMBER on GPUs. 2. Explicit Solvent Particle Mesh Ewald. Journal of Chemical Theory and Computation. 2013 in press.

44. Andersen HC. Rattle: A 'velocity' version of the shake algorithm for molecular dynamics calculations. J Comput Phys. 1983:52.

45. Darden T, York D, Pedersen L. Particle mesh Ewald: An N· log (N) method for Ewald sums in large systems. J Chem Phys. 1993; 98:10089–10092.

46. Humphrey W, Dalke A, Schulten K. VMD: visual molecular dynamics. J Mol Graph. 1996; 14:33–8. 27–8. [PubMed: 8744570]

47. Lutteke T, Frank M, von der Lieth CW. Carbohydrate Structure Suite (CSS): analysis of carbohydrate 3D structures derived from the PDB. Nucleic Acids Res. 2005; 33:D242–6. [PubMed: 15608187]

48. Bhattacharya A, Tejero R, Montelione GT. Evaluating protein structures determined by structural genomics consortia. Proteins. 2007; 66:778–95. [PubMed: 17186527]

49. Eisenberg D, Luthy R, Bowie JU. VERIFY3D: Assessment of protein models with three-dimensional profiles. Macromolecular Crystallography, Pt B. 1997; 277:396–404.

50. Sippl MJ. Recognition of Errors in 3-Dimensional Structures of Proteins. Proteins-Structure Function and Genetics. 1993; 17:355–362.

51. Laskowski RA, Macarthur MW, Moss DS, Thornton JM. Procheck - a Program to Check the Stereochemical Quality of Protein Structures. Journal of Applied Crystallography. 1993; 26:283–291.

52. Davis IW, Leaver-Fay A, Chen VB, Block JN, Kapral GJ, Wang X, Murray LW, Arendall WB, Snoeyink J, Richardson JS, Richardson DC. MolProbity: all-atom contacts and structure validation for proteins and nucleic acids. Nucleic Acids Research. 2007; 35:W375–W383. [PubMed: 17452350]

53. DeLano WL, Ultsch MH, de Vos AM, Wells JA. Convergent solutions to binding at a protein-protein interface. Science. 2000; 287:1279–83. [PubMed: 10678837]

Highlights

- IgG Fc exhibits large-scale domain motions

- Domain motions characterized by X-ray crystallography and 200ns MD simulations.

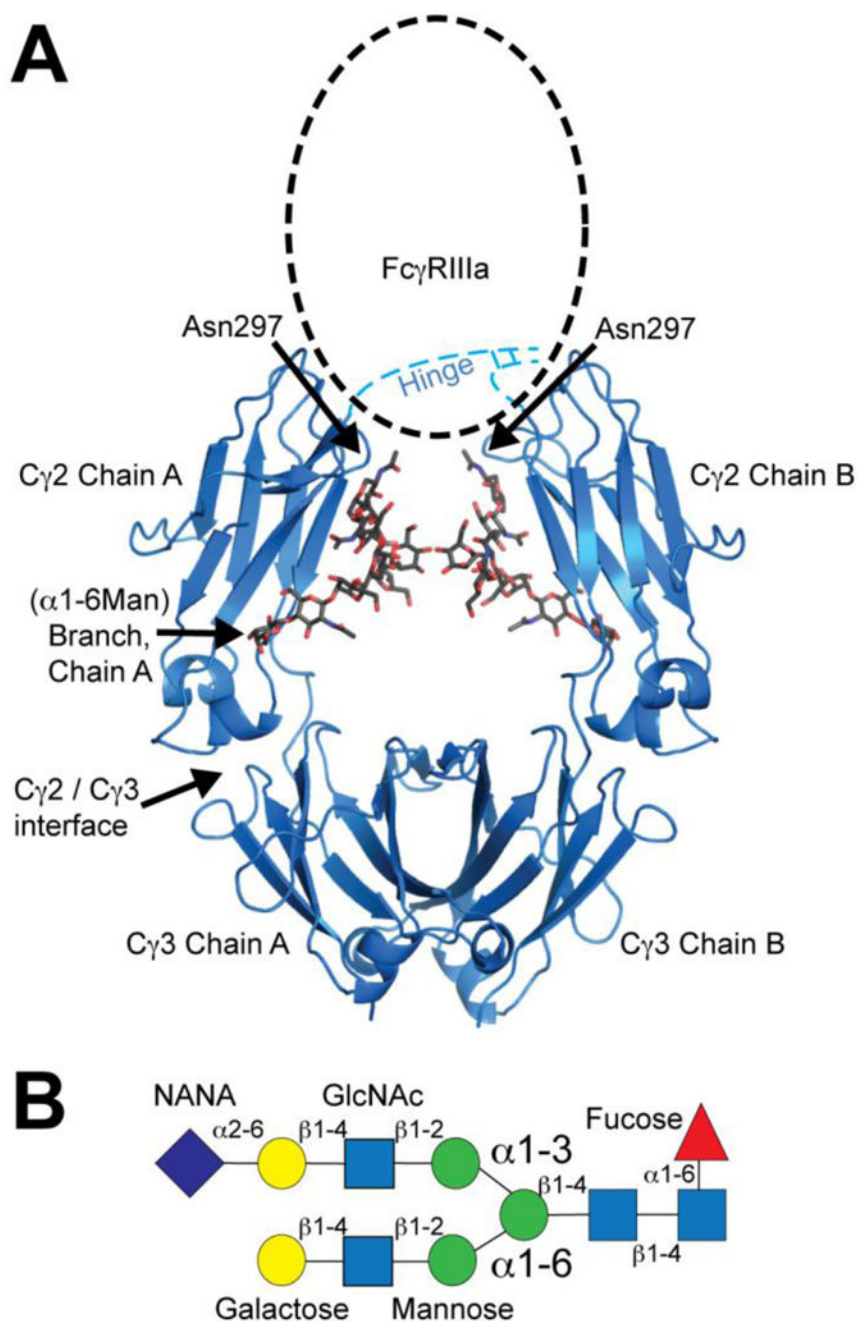- Inter-dimer Hinge and Fc domain interface residues limit motion.

Figure 1.
A structural model of the IgG1 Fc, determined by x-ray crystallography, is labeled to highlight Fc structural features (A). The hinge region, not resolved in this structure, is indicated in with dashed lines along with the previously identified Fcγ Receptor IIIa binding site [16; 17]. A cartoon shows a representative IgG1 Fc N-glycan and the conserved glycosidic linkages (B). GlcNAc: *N*-acetylglucosamine; NANA: *N*-acetylneuraminic acid. A G2F glycan, as studied here, would be identical to the glycan shown in (B) if the NANA residue were removed.
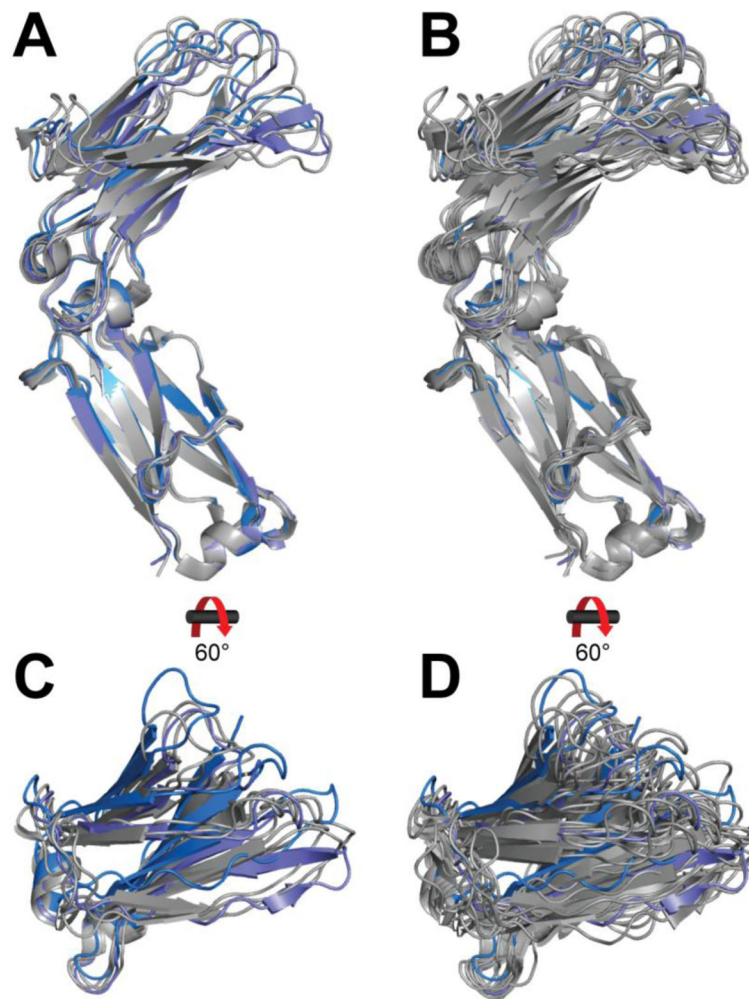
Figure 2.
A comparison of IgG1 Fc monomers highlights the positional diversity of the Cγ2 domains in Fc remodeled to the Gal-terminated glycoform (A) and rotated (C), or from a representative sampling of database structures (B and D). The structure reported herein is drawn in blue.
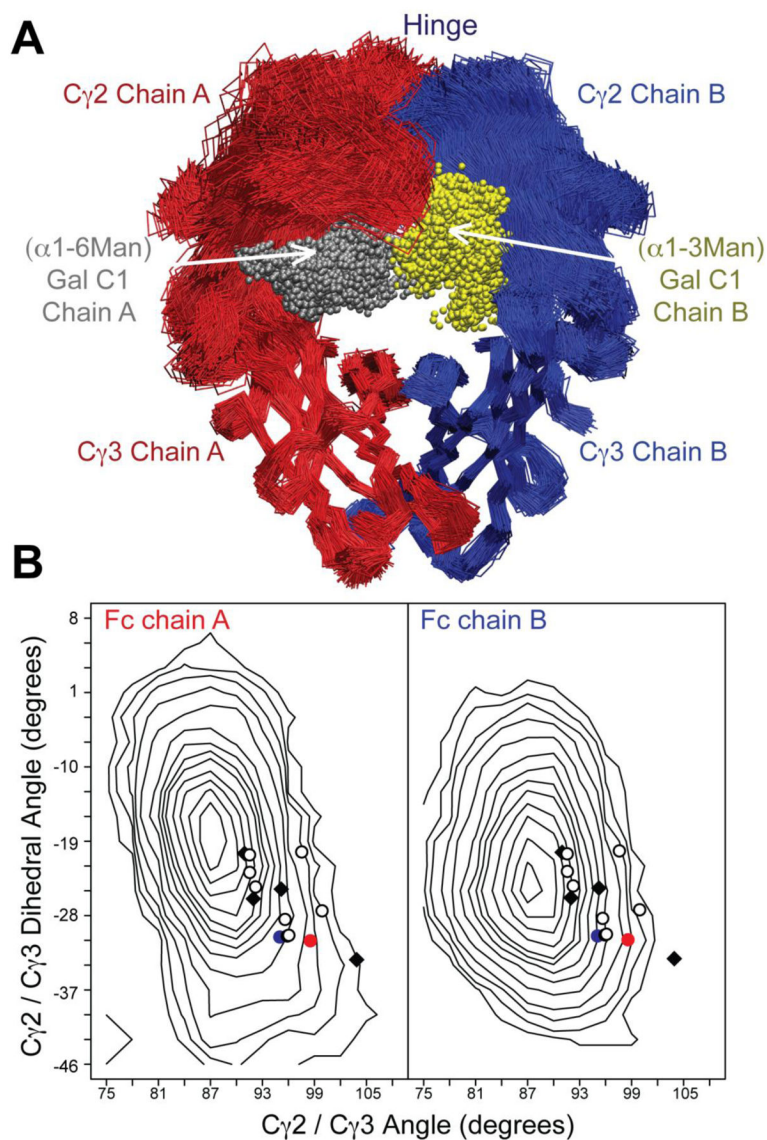
Figure 3.

(A) Snapshots from a 200 μs all-atom simulation of IgG1 Fc revealed considerable conformational heterogeneity of the Cγ2 domains. The position of Gal C1 atoms at each snapshot is shown with a sphere. (B) Two-dimensional histograms show the distribution of the Fc Cγ2/Cγ3 angle. Population distributions from the 200 ns molecular dynamics simulation are shown as contours, parameters from the x-ray structure reported here are shown as filled *red* (chain A) or *blue* (chain B) dots, similar x-ray structures containing Gal-terminated glycans or the Fc–FcγRIIIa complex are represented as open circles or black diamonds, respectively.
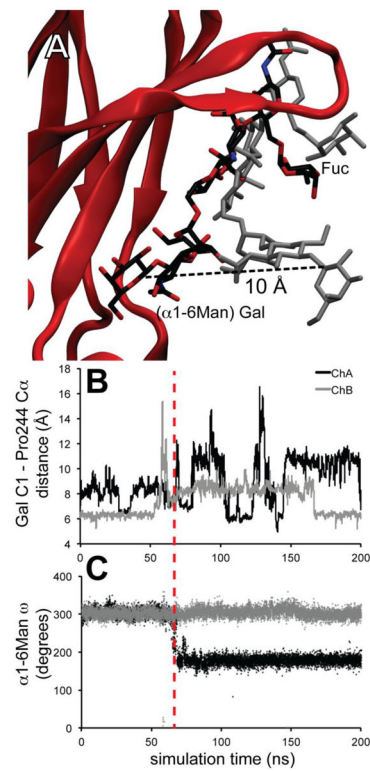
Figure 4.
The N-glycan from both chains exhibits reversible dissociation from the polypeptide surface. (A) An overlay of two N-glycan positions from Chain A, the unbound glycan is drawn as a *grey* stick model. (B) A plot of the Pro244 – Gal distance shows multiple states with the glycan bound and unbound to the polypeptide surface. (C) The ω torsion angle measurement of the αMan residue linked to the 6-position of the branch point βMan along the molecular dynamics trajectory. A dashed *red* line is used to denote the midpoint of the structural excursion for the chain A Man.
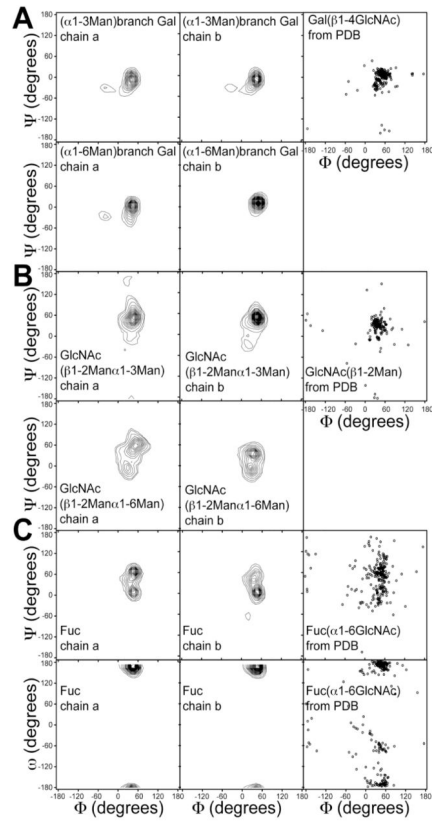
Figure 5.
Glycosidic torsion angle measurements (Φ, Ψ, ω) for the Gal (A), GlcNAc (B) and Fuc (C)
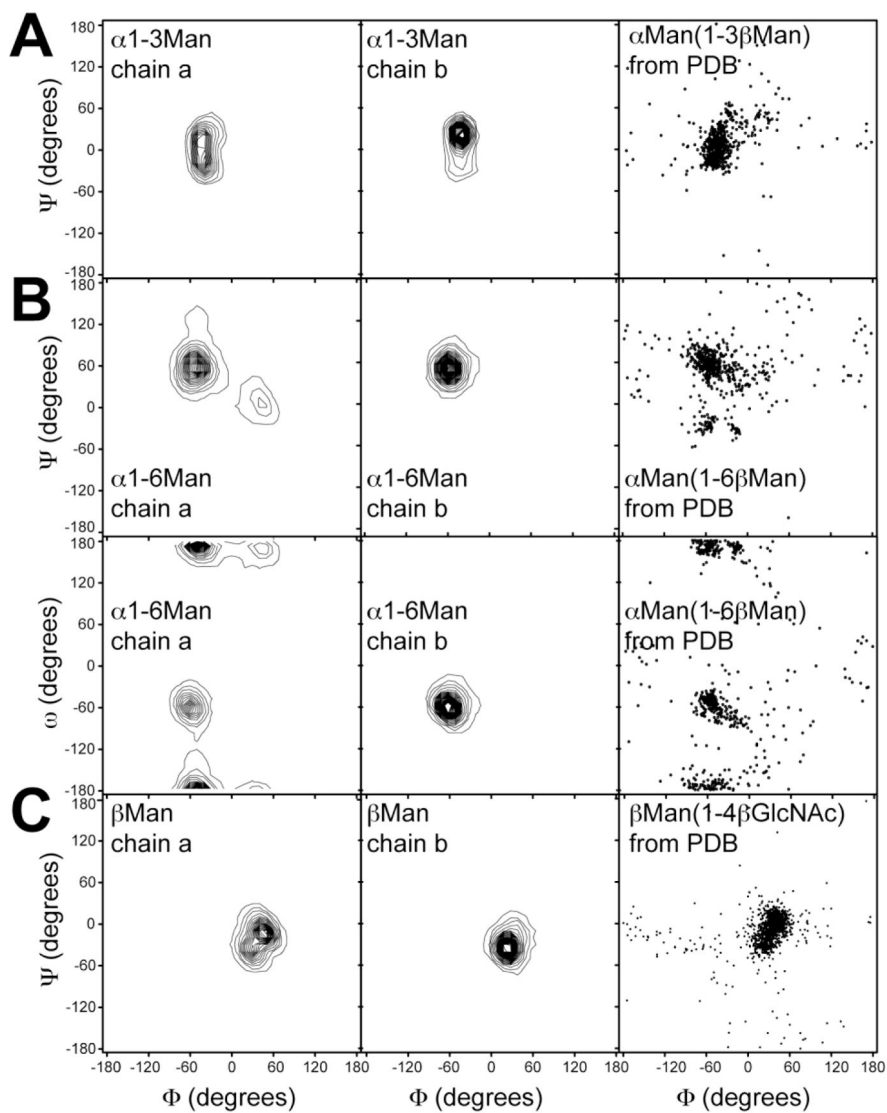residues. Measurements from models in the PDB are shown for comparison.

Figure 6.
Glycosidic torsion angle measurements for the α 1-3Man (A), α1-6Man (B) and βMan (C) residues. Measurements from models in the PDB are shown for comparison.
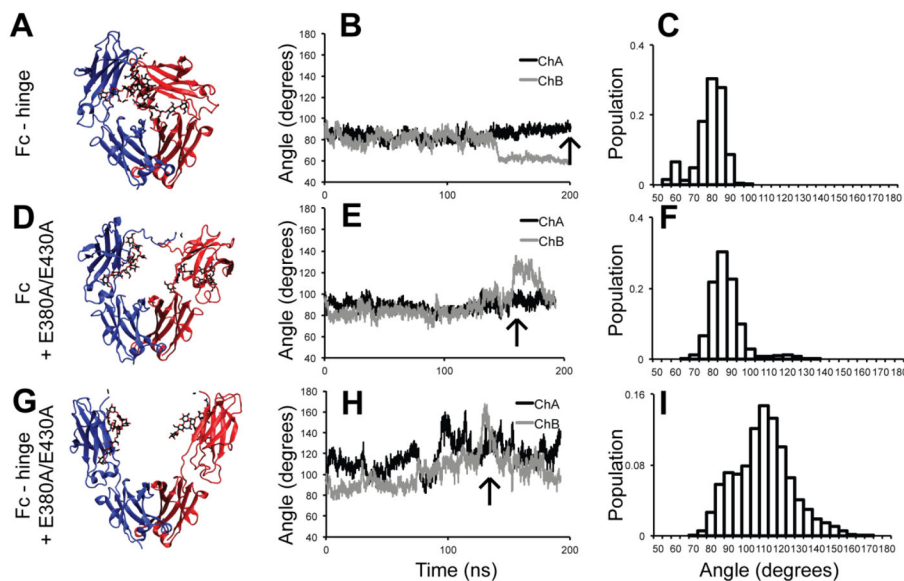
Figure 7.
Analysis of Fc amino acid mutations reveals multiple factors contribute to Cγ2 motion. A simulation of Fc with a truncated hinge region shows a limited increase in Cγ2 mobility from a snapshot (A), trajectory plot (B) and histogram (C) of the Cγ2 / Cγ3 angle. Likewise, mutating two Glu residues involved in stable salt bridges at the Cγ2 / Cγ3 interface has a limited affect (snapshot (D), trajectory plot (E) and histogram (F)). A simulation with combined hinge and interface mutations, however, exhibited a much greater range of Cγ2 positions (snapshot (G), trajectory plot (H) and histogram (I)). Vertical arrows below the trajectory plots indicate the points from which structural snapshots in the first column were taken.

Table 1

Summary of Crystallographic Information for IgG1 Fc

Space Group	$P2_12_12_1$
Molecules per asymmetric unit	2
Unit cell parameters	a=49.1 Å b=79.8 Å c=128.4 Å α=90 ° β=90 ° γ=90 °
Resolution[a]	67.82 - 1.90 (1.95 - 1.90) Å
Unique reflections	37848 (2326)
Completeness	98.3 (82.99) %
Redundancy	6
Rmerge	0.08
Rcryst	21.4 (27.3) %
Rfree	0.258 (0.292) %
No. of protein atoms	3350
No. of water molecules	149
Average B factor	31.7 Å^2
Protein chain A	32.8 Å^2
Protein chain B	30.6 Å^2
Carbohydrate residues (mono A/mono B)	66.9 / 46.5 Å^2
Water molecules	32.9 Å^2
rmsd	
Bond lengths	0.024 Å
Bond angles	1.9°
Ramachandran statistics	
Most favored region	94.2%
Allowed region	5.8%
Generously allowed	0.0%
PSVS Z-scores [48]	
Verify3D [49]	−1.12
Prosall [50]	−0.25
Procheck (phi-psi) [51]	−0.47
MolProbity [52]	0.01

[a]
values in parentheses are for the highest resolution shell

Table 2

Summary of IgG Fc Conformational Parameters

PDB Deposition	Chain	Cγ2/ Cγ3 Angle (°)	Cγ2 / Cγ3 Dihedral Angle (°)	Cγ2 / Cγ2 Inter Asn297 Distance (Å)	Res (Å)	Notes
herein: 4KU1	A B	98.5 95.1	−31.1 −30.6	29.1	1.9	G2F glycan
1H3V[19]	A B	96.0 91.5	−30.5 −20.7	33.3	3.1	G2F Glycan
1H3W[19]	-	99.9	−27.5	32.2	2.8	G2F, symmetric
1H3Y[19]	A B	95.7 97.6	−28.5 −20.4	22.8	4.1	unmodified glycan
1FC1[6]	A B	96.3 92.2	−30.4 −24.6	33.4	2.9	unmodified glycan
1L6X[53]	-	91.6	−22.8	31.9	1.65	Peptide-bound Gal visible
1E4K[16]	A B	92.0 103.9	−26.0 −33.4	36.2	3.2	Fc - FcγRIIIa complex
3AY4[17]	A B	95.2 91.0	−24.9 −20.5	33.5	2.2	Fc - FcγRIIIa complex
MD Range	-	75 to 108	−146 to 5.0	24 to 37		